Electronic Supplementary Material (ESI) for Inorganic Chemistry Frontiers.
This journal is © the Partner Organisations 2022

Electronic Supplementary Information

Experimental section

Materials: Sodium nitrate ($NaNO_3$, 99.0%), sodium nitrite ($NaNO_2$, 99.0%), ammonium chloride (NH_4Cl), sodium hydroxide (NaOH), sodium salicylate ($C_7H_5NaO_3$), trisodium citrate dihydrate ($C_6H_5Na_3O_7·2H_2O$), p–dimethylaminobenzaldehyde ($C_9H_{11}NO$), sodium nitroferricyanide dihydrate ($C_5FeN_6Na_2O·2H_2O$), 0.8 wt% sulfamic acid solution (H_3NO_3S) and sodium hypochlorite solution (NaClO) were purchased from Aladdin Ltd. (Shanghai, China). Cobalt nitrate hexahydrate ($Co(NO_3)_2·6H_2O$) was purchased from Chengdu Kelong Chemical Reagent Co. Ltd. Sulfuric acid (H_2SO_4), hydrogen peroxide (H_2O_2), hydrochloric acid (HCl), hydrazine monohydrate ($N_2H_4·H_2O$) and ethyl alcohol (C_2H_5OH) were bought from Beijing Chemical Corporation. (China). Ti plate (thickness is 0.2 mm) was purchased from Qingyuan Metal Materials Co., Ltd (Xingtai, China) and treated with 3 M HCl for 30 minutes before hydrothermal reaction. All chemicals used in this work were analytical grade and direct use without further purification.

Preparation of Co-TiO_2/TP: Firstly, Ti plates were cut into small pieces (2.0 × 4.0 cm^2) and sonicated in acetone, ethanol, and distilled water for 15 min, respectively. After then, they were put into 40 mL of 5 M NaOH aqueous solution in a 50 mL Teflon-lined autoclave. The autoclave was kept in an electric oven at 180°C for 24 h. After the autoclave was cooled down naturally to room temperature, the samples were moved out, washed with deionized water and ethanol several times and dried at 60 °C for 30 min. Then the resulting $Na_2Ti_2O_5$/TP was immersed in 0.25 M $Co(NO_3)_2$ for 1 h to exchange Na^+ with Co^{2+}. The resulting $CoTi_2O_5·H_2O$/TP was rinsed with deionized water and ethanol several times and dried at 60 °C for 30 min. Subsequently, $CoTi_2O_5·H_2O$/TP was annealed in a tube furnace at 500°C under an Ar atmosphere for 2 hours. After cooling to room temperature, Co-TiO_2/TP was finally obtained.

Preparation of TiO_2/TP: Firstly, Ti plates were cut into small pieces (2.0 × 4.0 cm^2)

and sonicated in acetone, ethanol, and distilled water for 15 min, respectively. After then, they were put into 40 mL of 5 M NaOH aqueous solution in a 50 mL Teflon-lined autoclave. The autoclave was kept in an electric oven at 180℃ for 24 h. After the autoclave was cooled down naturally to room temperature, the samples were moved out, washed with deionized water and ethanol several times and dried at 60 ℃ for 30 min. Then the resulting $Na_2Ti_2O_5$/TP was immersed in 1 M HCl for 1 h to exchange Na^+ with H^+. The as-prepared $H_2Ti_2O_5 \cdot H_2O$/TP was rinsed with deionized water and ethanol several times and dried at 60 ℃ for 30 min. Subsequently, $H_2Ti_2O_5 \cdot H_2O$/TP was annealed in a tube furnace at 500°C under an Ar atmosphere for 2 hours. After cooling to room temperature, TiO_2/TP was finally obtained.

Characterizations: XRD data were acquired by a LabX XRD–6100 X-ray diffractometer with a Cu Kα radiation (40 kV, 30 mA) of wavelength 0.154 nm (SHIMADZU, Japan). SEM measurements were carried out on a GeminiSEM 300 scanning electron microscope (ZEISS, Germany) at an accelerating voltage of 5 kV. XPS measurements were performed on an ESCALABMK II X-ray photoelectron spectrometer using Mg as the exciting source. The absorbance data of the spectrophotometer was measured on a UV-Vis spectrophotometer. TEM image was obtained from a Zeiss Libra 200FE transmission electron microscope operated at 200 kV. Gas chromatography (GC-2014C, SHIMADZU) was utilized to quantitatively detect H_2 and N_2. ^{1}H NMR spectra were collected on Varian VNMRS 600 MHz (the USA).

Electrochemical measurements: All electrochemical measurements were carried out on the CHI660E electrochemical workstation (Shanghai, Chenhua) using a standard three-electrode setup. The electrolyte solution was Ar-saturated of 0.1 M NaOH with 0.1 M NO_3^-, using Co-TiO_2/TP, TiO_2/TP, or TP as the working electrode, a graphite rod as the counter electrode, and a Hg/HgO as the reference electrode. We use an H-type electrolytic cell separated by a Nafion 117 membrane which was protonated by boiling in ultrapure water, H_2O_2 (5%) aqueous solution and 0.5 M H_2SO_4 at 80 °C for another 2 h, respectively. All the potentials reported in our work were converted to a reversible hydrogen electrode via calibration with the following equation: E (RHE) =

E (Hg/HgO) + (0.098 + 0.0591 × pH) V and the presented current density was normalized to the geometric surface area.

Determination of NH_3: The concentration of produced NH_3 was determined by spectrophotometry measurement with the indophenol blue method (the obtained electrolyte was diluted 40 times).[1] In detail, 2 mL of the diluted catholyte was obtained from the cathodic chamber and mixed with 2 mL of a 1 M NaOH solution that contained salicylic acid and sodium citrate. Then, 1 mL of 0.05 M NaClO and 0.2 mL of 1 wt% $C_5FeN_6Na_2O$ were dropped into the collected electrolyte solution. After standing at room temperature for 2 h, the ultraviolet-visible absorption spectrum was measured. The concentration-absorbance curve was calibrated using the standard NH_4Cl solution with NH_3 concentrations of 0, 0.25, 0.5, 1.5, 2.0,3.0 and 4.0 μg mL^{-1} in 0.1 M NaOH. The absorbance at 655 nm was measured to quantify the NH_3 concentration using standard NH_4Cl solutions ($y = 0.42074\ x + 0.02455$, $R^2 = 0.9997$).

Determination of NO_2^-: The NO_2^- concentration was analyzed using the Griess test.[2] The Griess reagent was prepared by dissolving 0.1 g N–(1–naphthyl) ethylenediamine dihydrochloride, 1.0 g sulfonamide and 2.94 mL H_3PO_4 in 50 mL deionized water. In a typical colourimetric assay, the 1.0 mL Griess reagent was mixed with the 1.0 mL nitrite-containing solution and 2.0 mL H_2O and allowed to react at room temperature for 10 min, in which sulfonamide reacts with NO_2^- to form a diazonium salt and then further reacts with the amine to form an azo dye (magenta). The absorbance at 540 nm was measured to quantify the NO_2^- concentration with a standard curve of NO_2^- ($y = 0.20595\ x + 0.06651$, $R^2 = 0.9999$).

Determination of N_2H_4: In this work, we used the method of Watt and Chrisp[3] to determine the concentration of produced N_2H_4. The chromogenic reagent was a mixed solution of 5.99 g $C_9H_{11}NO$, 30 mL HCl and 300 mL C_2H_5OH. In detail, 1 mL of electrolyte was added into 1 mL prepared colour reagent and stirred for 15 min in the dark. The absorbance at 455 nm was measured to quantify the N_2H_4 concentration with a standard curve of hydrazine ($y = 0.6878\ x + 0.1066$, $R^2 = 0.9997$).

Detection of Co^{2+}: First, the Co-TiO_2 nanoribbons array was scraped from the TP and weighed 40 mg. Next, the Co-TiO_2 powder was dissolved into 2 mL of mixed acid

prepared from hydrochloric acid and nitric acid (V_{HCl}: V_{HNO3} = 3:1). Finally, the prepared solution was diluted 20,000-fold and the concentration of Co ions was measured on an inductively coupled plasma-mass spectrometry (ICP-MS) instrument.

Calculations of FE and NH_3 yield:

The amount of NH_3 (m_{NH3}) was calculated by the following equation:

$$m_{NH3} = [NH_3] \times V$$

FE of NH_3 formation was calculated by the following equation:

$$FE = (8 \times F \times [NH_3] \times V) / (M_{NH3} \times Q) \times 100\%$$

The NH_3 yield rate is calculated using the following equation:

$$NH_3 \text{ yield} = ([NH_3] \times V) / (M_{NH3} \times t \times A)$$

Where F is the Faradaic constant (96485 C mol^{-1}), $[NH_3]$ is the NH_3 concentration, V is the volume of electrolyte in the anode compartment (70 mL), M_{NH3} is the molar mass of the NH_3 molecule, Q is the total quantity of applied electricity; t is the electrolysis time (1 h) and A is the geometric area of the working electrode (1 × 1 cm^2).

Calculation of the partial current density:

$$j_{partial} = FE \times I$$

Among them, $j_{partial}$ represents the partial current density at each given potential; FE is the corresponding Faradaic efficiency of each product at the given potential; I is the corresponding current at each given potential.

Calculation of the energy consumed in the formation of V_{Os} (E_f):

The energy consumed to form V_{Os} in Co-TiO_2 can be calculated by the following equation:

$$E_f = E_{(VOs\text{-}Co\text{-}TiO2)} + E_{(O2)}/2 - E_{(Co\text{-}TiO2)}.$$

Among them, $E_{(VOs\text{-}Co\text{-}TiO2)}$ denotes the total energy of the Co-TiO_2 system after the formation of V_{Os}; $E_{(O2)}$ is the energy of the O_2 molecule; $E_{(Co\text{-}TiO2)}$ refers to the total energy of the TiO_2 system after Co doping into TiO_2.

The energy consumed to form V_{Os} in TiO_2 can be calculated by the following equation:

$$E_f = E_{(VOs\text{-}TiO2)} + E_{(O2)}/2 - E_{(TiO2)}.$$

Among them, $E_{(VOs\text{-}TiO2)}$ presents the total energy of TiO_2 after the formation of V_{Os}; $E_{(O2)}$ is the energy of the O_2 molecule; $E_{(TiO2)}$ represents the total energy of the TiO_2 system without $V_{Os.}$

DFT calculations details: First-principles calculations with spin-polarized were performed using density functional theory (DFT) implemented in the VASP package,[4] and the projector augmented wave (PAW) approach was used to describe the interaction between ionic core and valence electrons with a cutoff of 500 eV.[5] Perdew-Burke-Ernzerhof functional (PBE) with semi-empirical corrections of DFT-D3 were employed to depict the exchange-correlation functional effect by general gradient approximation (GGA).[6] Co-TiO_2 (101) and TiO_2 (101) surfaces with two terminations were modelled. The bottom two layers were fixed, and the upper two layers were permitted to relax. The thickness of the vacuum region is 15 Å to avert spurious interaction. The Brillouin zone was built by 3 × 3 × 1 special k-points based on the Monkhorst Pack scheme for structural configuration optimizations.[7] The total energy is less than 10^{-5} eV and the force convergence threshold is 0.02 eV/Å, respectively. The DFT calculation results were analyzed by VASPKIT software.[8]

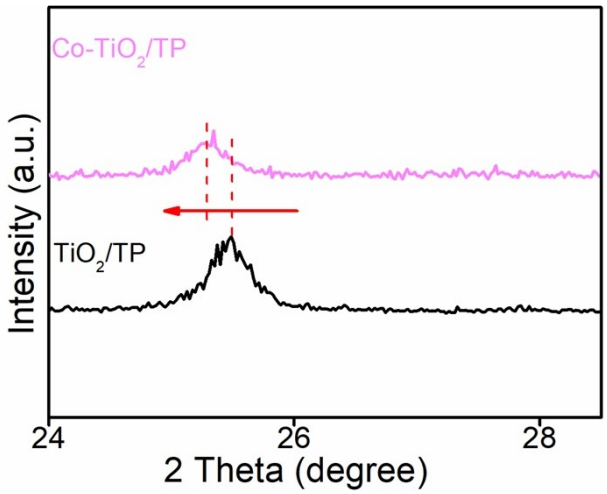

Fig. S1. XRD patterns for Co-TiO_2/TP and TiO_2/TP.

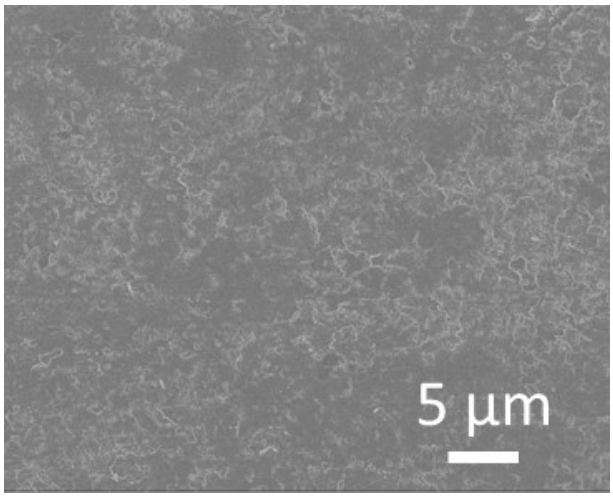

Fig. S2. SEM image of bare TP

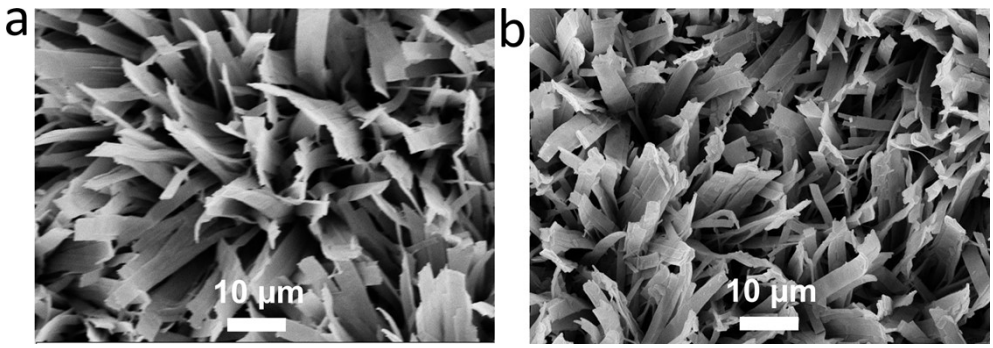

Fig. S3. SEM images of (a) $Na_2Ti_2O_5$/TP and (b) $CoTi_2O_5$/TP.

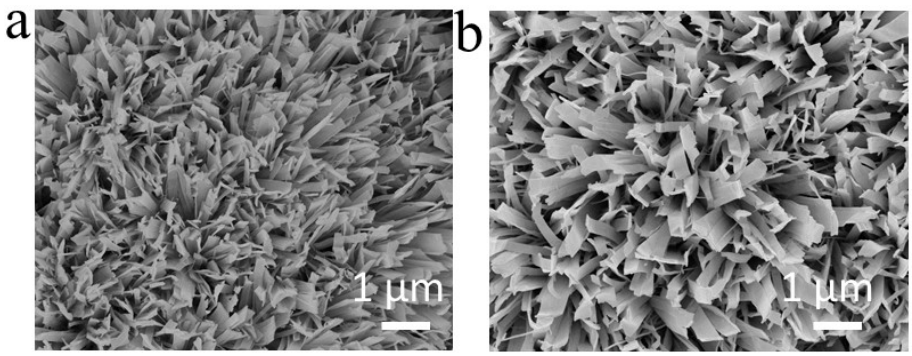

Fig. S4. SEM images of (a) TiO_2/TP, and (b) Co-TiO_2/TP.

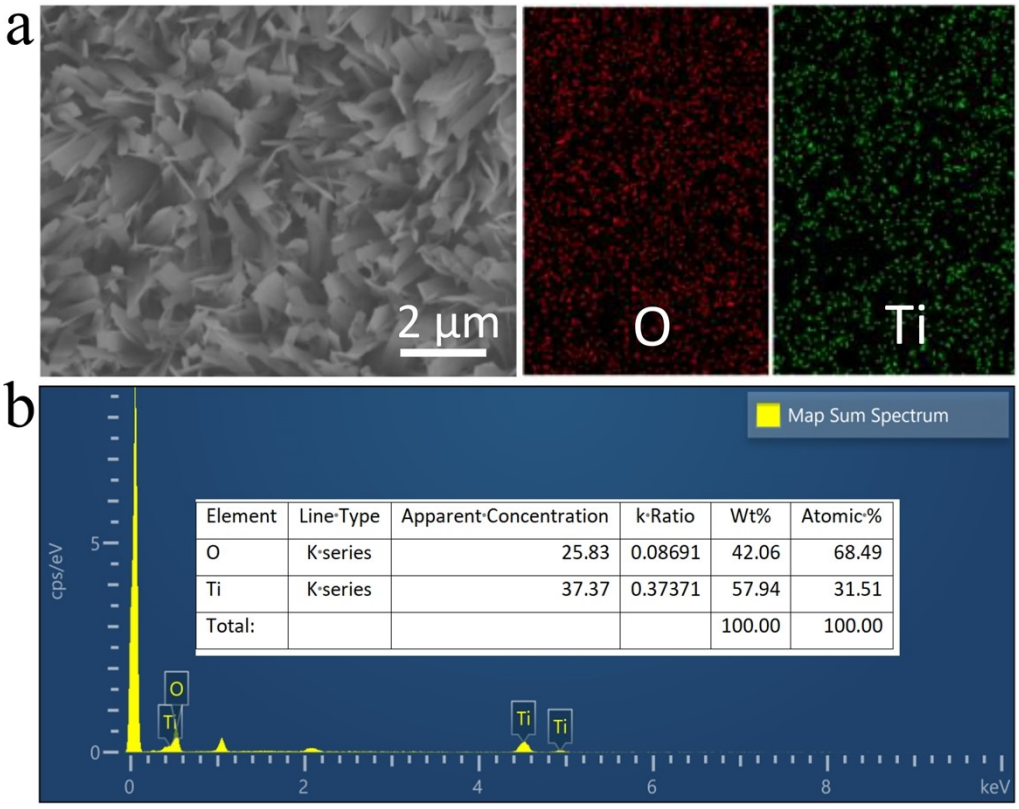

Element	Line Type	Apparent Concentration	k Ratio	Wt%	Atomic %
O	K series	25.83	0.08691	42.06	68.49
Ti	K series	37.37	0.37371	57.94	31.51
Total:				100.00	100.00

Fig. S5. (a) The SEM and corresponding EDX mapping images of Ti and O for TiO_2/TP. (b) EDX spectrum of TiO_2/TP.

a

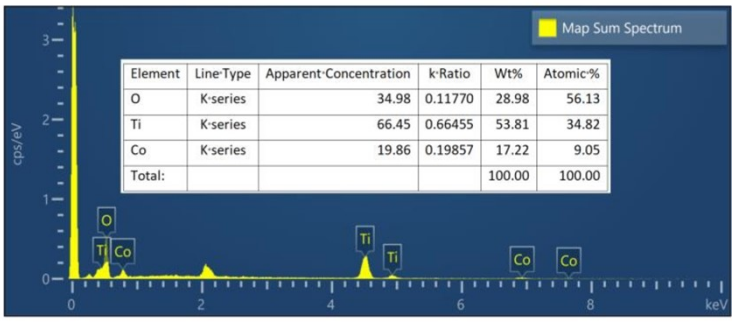

Element	Line Type	Apparent Concentration	k Ratio	Wt%	Atomic %
O	K series	34.98	0.11770	28.98	56.13
Ti	K series	66.45	0.66455	53.81	34.82
Co	K series	19.86	0.19857	17.22	9.05
Total:				100.00	100.00

b

			59 Co [He]	59 Co [He]
2		**Standard sample number**	**Standard concentration[ppb]**	**CPS**
3	BlkVrfy			377.0533333
4	CalBlk	0	0	47937.65333
5	CalStd	0.1	0.312710288	82204.67667
6	CalStd	1	1.461573388	208097.94
7	CalStd	10	10.28932874	1175449.863
8	CalStd	100	103.4255127	11381381.4
9	CalStd	1000	999.6540726	109590766.1
10		**Test sample number**		
11	Sample	1	31.59290893	3509911.847
12	Sample	2	31.72994938	3524928.84
13	Sample	3	31.85316011	3538430.363

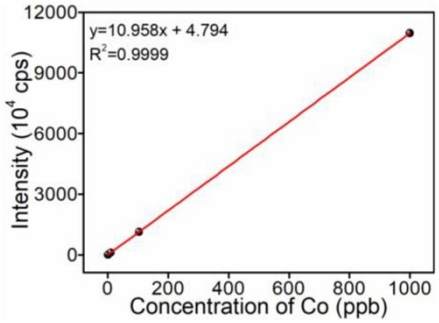

Fig. S6. (a) EDX spectrum for Co-TiO_2/TP. (b) The ICP-MS data of Co ions and calibration curve.

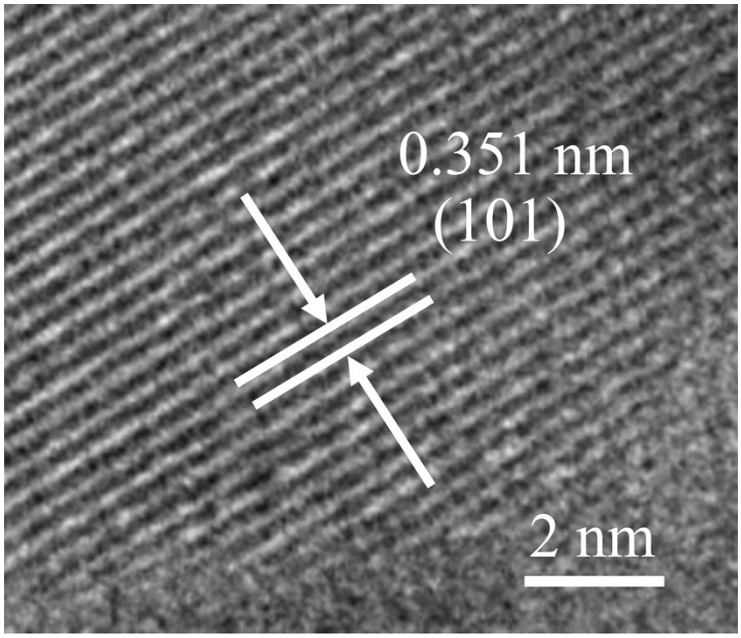

Fig. S7. HRTEM image of undoped TiO_2

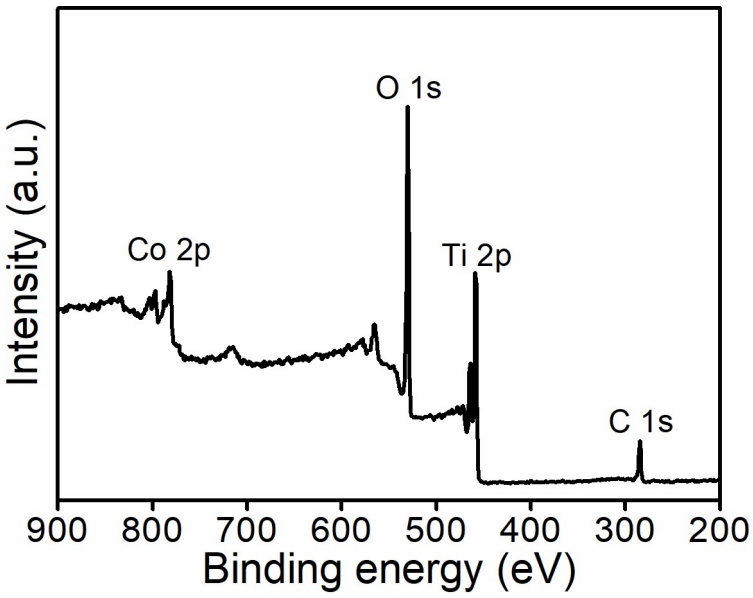

Fig. S8. XPS survey spectrum of Co-TiO_2.

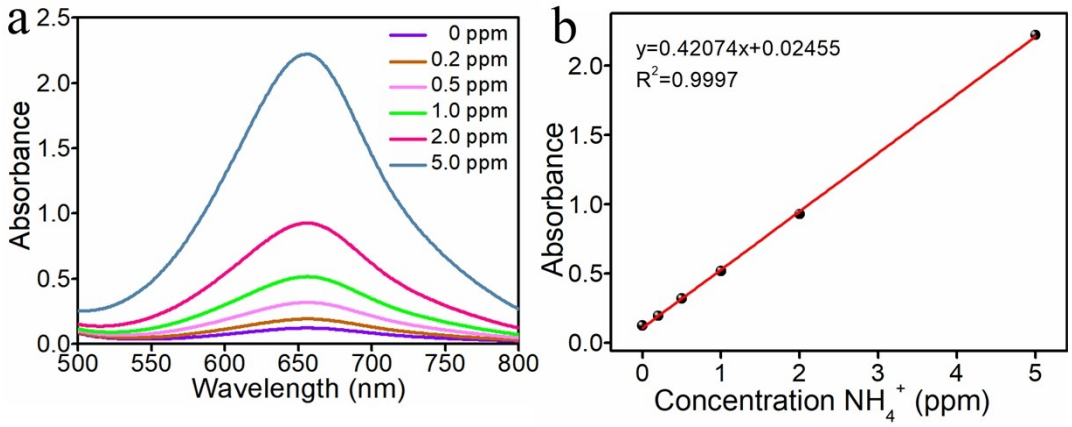

Fig. S9. (a) UV-Vis absorption spectra of indophenol assays kept with different concentrations of NH_4^+ after incubated for 2 h at room temperature. (b) Calibration curve used for estimation of NH_4^+ concentration.

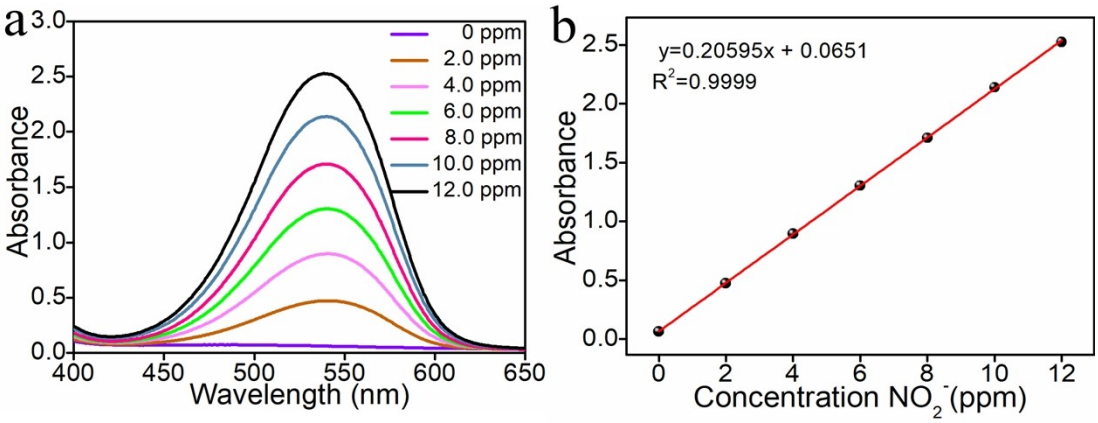

Fig. S10. UV-Vis absorption spectra of various NO_2^- concentrations after incubated for 10 min at room temperature. (b) Calibration curve used for quantification of NO_2^- concentration.

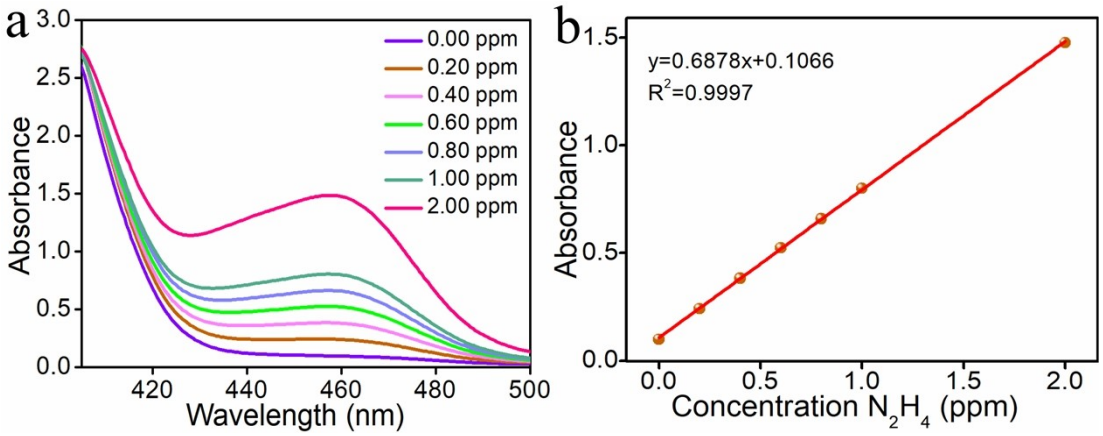

Fig. S11. (a) UV-Vis absorption spectra of various N_2H_4 concentrations after incubated for 15 min at room temperature. (b) Calibration curve used for calculation of N_2H_4 concentration.

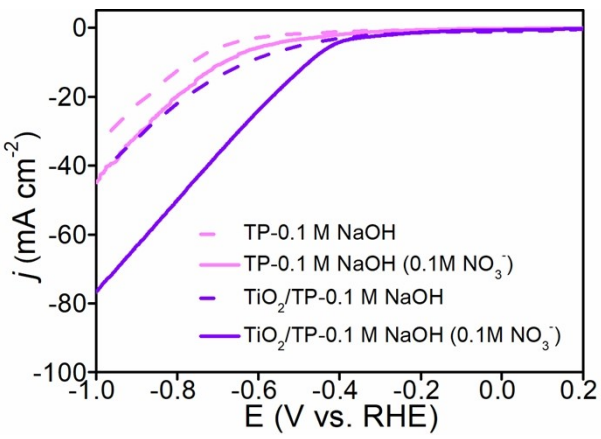

Fig. S12. LSV curves of TiO_2/TP and TP in 0.1 M NaOH with and without 0.1 M NO_3^-.

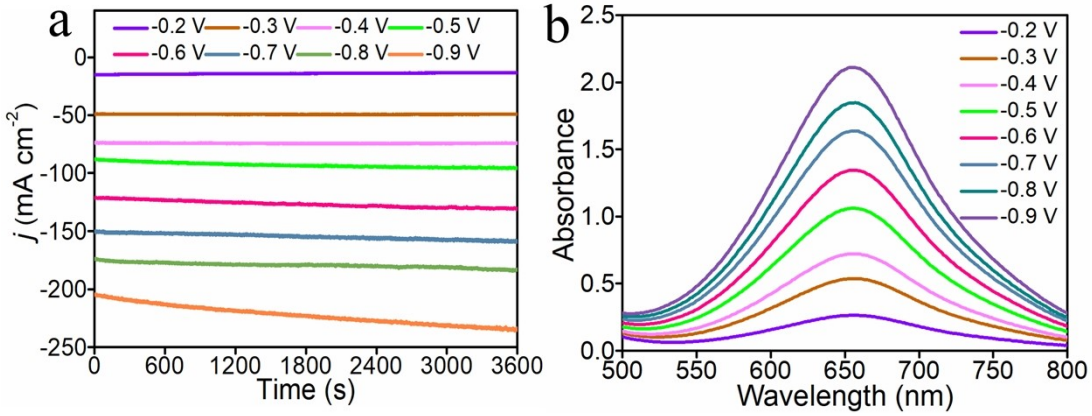

Fig. S13. (a) Chronoamperometry curves and (b) corresponding UV-Vis spectra of Co-TiO_2/TP at different given potentials.

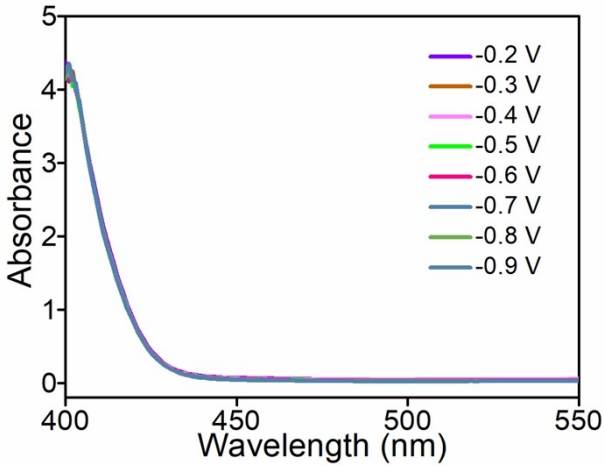

Fig. S14. UV-Vis absorption spectra of the electrolytes estimated by the method of Watt and Chrisp for the calculation of N_2H_4 concentration.

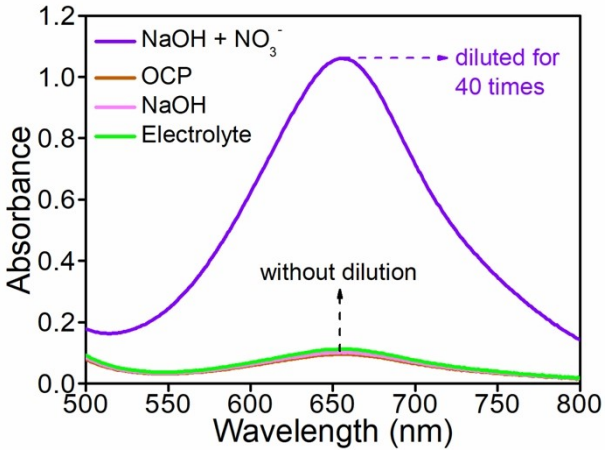

Fig. S15. UV-Vis absorption spectra of NH_3 concentrations at different conditions.

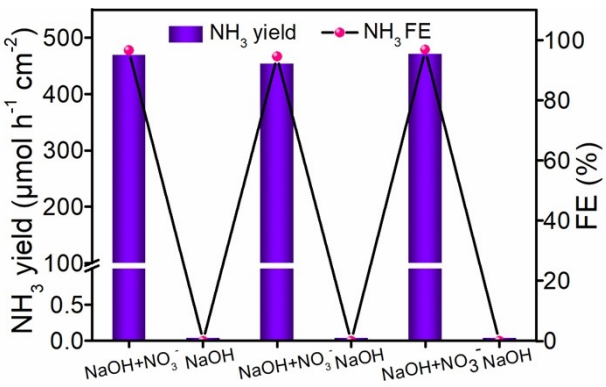

Fig. S16. NH_3 yields and FEs of Co-TiO_2/TP during the alternating cycle tests between NO_3^--containing and NO_3^--free 0.1 M NaOH solution.

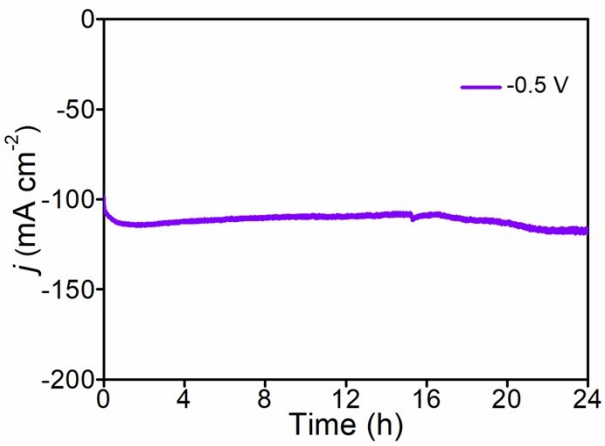

Fig. S17. Long-term stability test at –0.5 V.

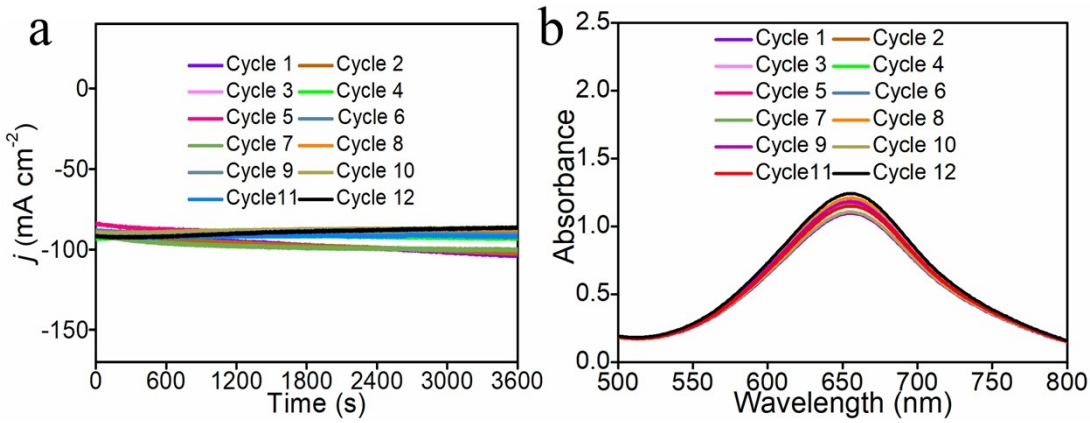

Fig. S18. (a) Chronoamperometry curves and (b) corresponding UV-Vis absorption spectra of Co-TiO_2/TP for electrogenerated NH_3 during cycling tests at –0.5 V.

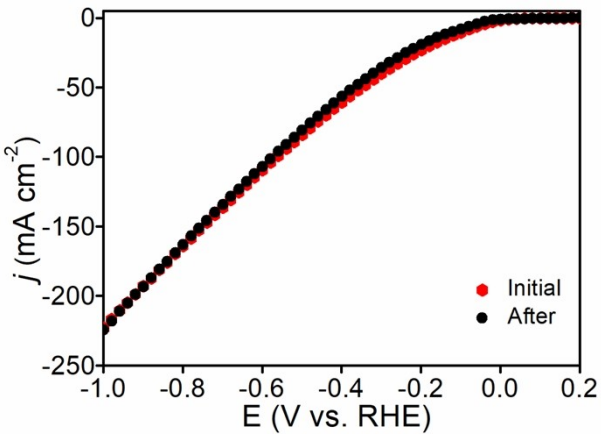

Fig. S19. LSV curves of Co-TiO_2/TP before and after 24-h electrolysis.

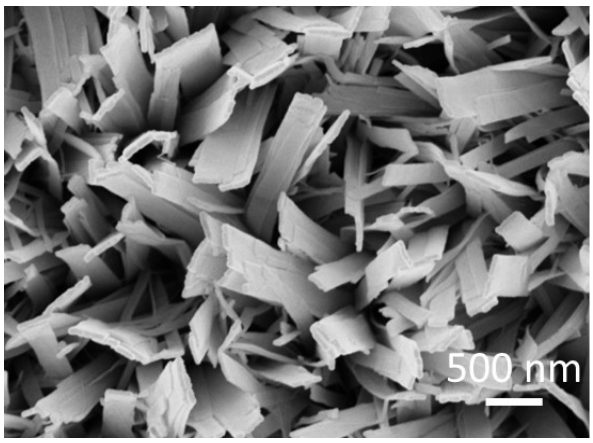

Fig. S20. SEM image of Co-TiO_2/TP after 24-h electrolysis.

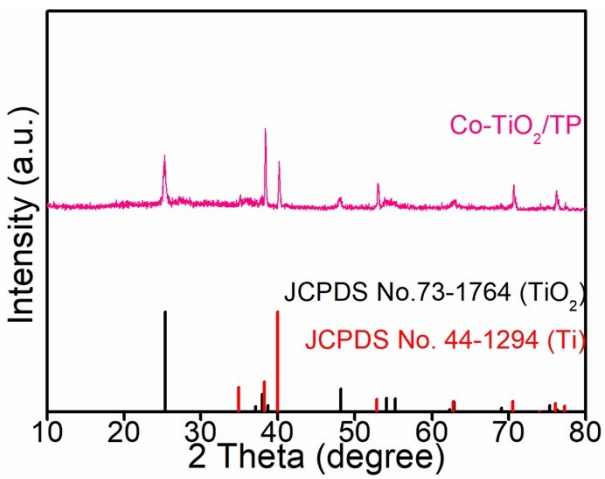

Fig. S21. XRD pattern of Co-TiO_2/TP after 24-h electrolysis.

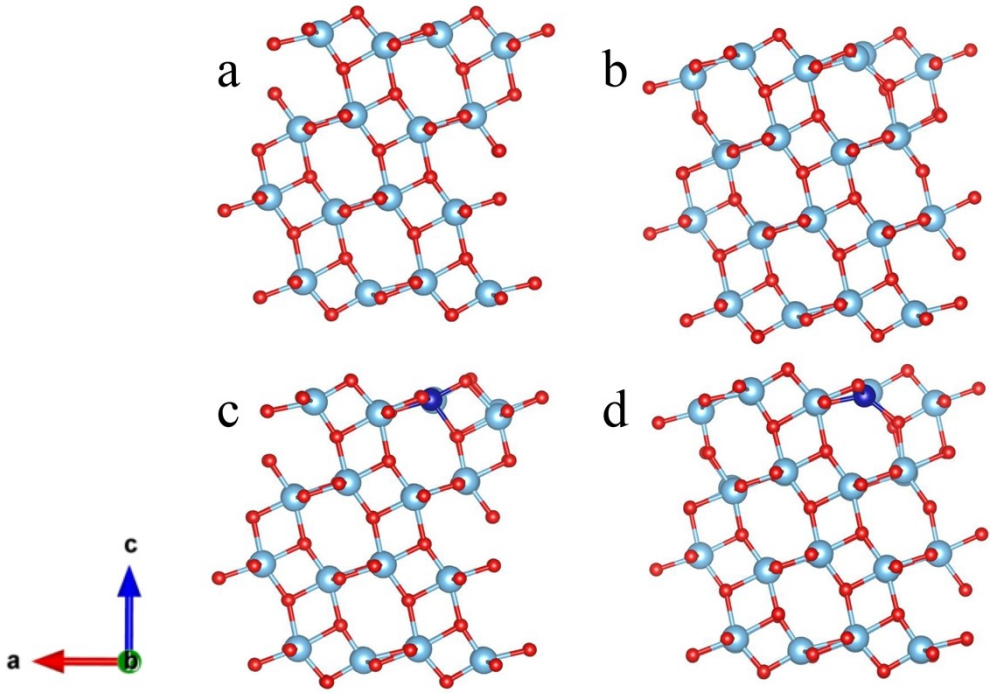

Fig. S22. Crystal structures of (a) TiO_2 without oxygen vacancies, (b) TiO_2 with oxygen vacancies, (c) Co-TiO_2 without oxygen vacancies, and (d) Co-TiO_2 with oxygen vacancies. Dark blue, red, and light blue spheres denote the Co, O, and Ti atoms, respectively.

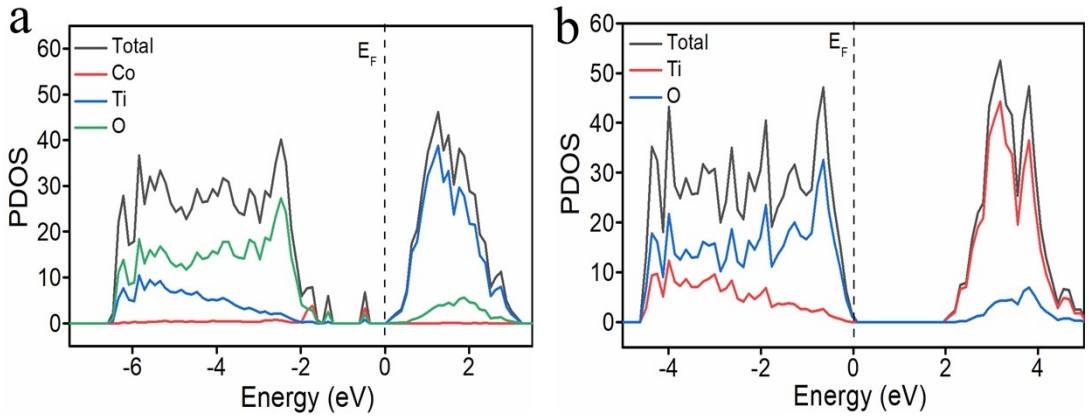

Fig. S23. Calculated PDOS of (a) Co-TiO_2 and (b) TiO_2 configuration.

Table S1. Comparison of catalytic performance of Co-TiO_2/TP with other reported NO_3RR electrocatalysts.

Catalyst	Electrolyte	NH_3 yield	FE	Ref.
Co-TiO_2/TP	0.1 M NaOH (0.1 M NO_3^-)	1127 μmol h^{-1} cm^{-2}	98.2%	This work
TiO_{2-x}	0.5 M Na_2SO_4 (50 ppm NO_3^-)	45 μmol h^{-1} $mg_{cat.}^{-1}$	85%	9
Pd facets	0.1 M NaOH (20 mM NO_3^-)	18 μmol h^{-1} cm^{-2}	35%	10
Ni NP	1 M NaOH (20 mM NO_3^-)	/	46.3%	11
Pd/TiO_2	0.5 M NaOH (0.25 M NO_3^-)	66 μmol h^{-1} cm^{-2}	92%	12
Cu	1 M NaOH (0.1 M NO_3^-)	/	79%	13
In–S–G	1 M KOH (0.1 M NO_3^-)	220 μmol h^{-1} $mg_{cat.}^{-1}$	75%	14
Fe SAC	1 M KOH (0.1 M NO_3^-)	/	86%	15
BC_2N/Pd	0.1 M KOH (0.25 M NO_3^-)	100 μmol h^{-1} cm^{-2}	97.42%	16
Fe–PPy SACs	0.1 M KOH (0.1 M NO_3^-)	160 μmol h^{-1} cm^{-2}	~100%	17
BCN@Ni	0.1 M KOH (0.1 M NO_3^-)	140 μmol h^{-1} cm^{-2}	91.15%	18
Ni_3B@$NiB_{2.74}$	0.1 M KOH (0.1 M NO_3^-)	200 μmol h^{-1} cm^{-2}	~100%	19
BCN-Cu	0.1 M KOH (100 mM NO_3^-)	110 μmol h^{-1} cm^{-2}	98.23%	20
$ZnCo_2O_4$	0.1 M KOH (0.1 M NO_3^-)	120 μmol h^{-1} $mg_{cat.}^{-1}$	95.4%	21
Co-NCNT	0.1 M NaOH (0.1 M NO_3^-)	350 μmol h^{-1} $mg_{cat.}^{-1}$	92%	22
$Cu_{50}Ni_{50}$	0.1 M NaOH (10 mM NO_3^-)	/	84 ± 2%	23

References

1 D. Zhu, L. Zhang, R. E. Ruther and R. J. Hamers, Photo-illuminated diamond as a solid-state source of solvated electrons in water for nitrogen reduction, *Nat. Mater.,* 2013, **12**, 836–841.

2 G. W. Watt and J. D. Chrisp, Spectrophotometric method for determination of hydrazine, *Anal. Chem.,* 1952, **24**, 2006–2008.

3 L. C. Green, D. A. Wagner, J. Glogowski, P. L. Skipper, J. S. Wishnok and S. R. Tannenbaum, Analysis of nitrate, nitrite, and [^{15}N] nitrate in biological fluids, *Anal. Biochem.*, 1982, **126**, 131–138.

4 G. Kresse and J. Hafner, Ab initio molecular-dynamics simulation of the liquid-metal–amorphous-semiconductor transition in germanium, *Phys. Rev. B,* 1994, **49**, 14251−14269.

5 G. Kresse and D. Joubert, From ultrasoft pseudopotentials to the projector augmented-wave method, *Phys. Rev. B,* 1999, **59**, 1758−1775.

6 J. P. Perdew, K. Burke and M. Ernzerhof, Generalized Gradient Approximation Made Simple, *Phys. Rev. Lett.,* 1996, **77**, 3865−3868.

7 H. J. Monkhorst and J. D. Pack, Special points for Brillouin-zone integrations, *Phys. Rev. B,* 1976, **13**, 5188−5192.

8 V. Wang, N. Xu, J. Liu, G. Tang and W. Geng, VASPKIT: A user-friendly interface facilitating high-throughput computing and analysis using VASP code, *Comput. Phys. Commun.,* 2021, **267**, 108033.

9 R. Jia, Y. Wang, C. Wang, Y. Ling, Y. Yu and B. Zhang, Boosting selective nitrate electroreduction to ammonium by constructing oxygen vacancies in TiO_2, *ACS Catal.,* 2020, **10,** 3533−3540.

10 J. Lim, C. Liu, J. Park, Y. Liu, T. P. Senftle, S. W. Lee and M. C. Hatzell, Structure sensitivity of Pd facets for enhanced electrochemical nitrate reduction to ammonia, *ACS Catal.,* 2021, **11**, 7568–7577.

11 L. Mattarozzi, S. Cattarin, N. Comisso, P. Guerriero, M. Musiani, L. Vázquez-Gómez and E. Verlato, Electrochemical reduction of nitrate and nitrite in alkaline media at CuNi alloy electrodes, *Electrochim. Acta*, 2013, **89**, 488–496.

12 Y. Guo, R. Zhang, S. Zhang, Y. Zhao, Q. Yang, Z. Huang, B. Dong and C. Zhi, Pd doping-weakened intermediate adsorption to promote electrocatalytic nitrate reduction on TiO_2 nanoarrays for ammonia production and energy supply with zinc–nitrate batteries, *Energy Environ. Sci.,* 2021, **14**, 3938–3944.

13 D. Reyter, G. Chamoulaud, D. Bélanger and L. Roué, Electrocatalytic reduction of nitrate on copper electrodes prepared by high-energy ball milling, *J. Electroanal. Chem.,* 2006, **596**, 13–24.

14 F. Lei, W. Xu, J. Yu, K. Li, J. Xie, P. Hao, G. Cui and B. Tang, Electrochemical synthesis of ammonia by nitrate reduction on indium incorporated in sulfur doped graphene, *Chem. Eng. J.,* 2021, **426**, 131317.

15 Z. Wu, M. Karamad, X. Yong, Q. Huang, D. A. Cullen, P. Zhu, C. Xia, Q. Xiao, M. Shakouri, F. Chen, J. Y. Kim, Y. Xia, K. Heck, Y. Hu, M. S. Wong, Q. Li, I. Gates, S. Siahrostami and H. Wang, Electrochemical ammonia synthesis via nitrate reduction on Fe single atom catalyst, *Nat. Commun.*, 2021, **12**, 2870.

16 X. Li, X. Zhao, Y. Zhou, J. Hu, H. Zhang, X. Hu and G. Hu, Pd nanocrystals embedded in BC_2N for efficient electrochemical conversion of nitrate to ammonia, *Appl. Surf. Sci.*, 2022, **584**, 152556.

17 P. Li, Z. Jin, Z. Fang and G. Yu, A single-site iron catalyst with preoccupied active centers that achieves selective ammonia electrosynthesis from nitrate, *Energy Environ. Sci.*, 2021, **14**, 3522–3531.

18 X. Zhao, Z. Zhu, Y. He, H. Zhang, X. Zhou, W. Hu, M. Li, S. Zhang, Y. Dong, X. Hu, A. V. Kuklin, G. V. Baryshnikov, H. Ågren, T. Wågberg and G. Hu, Simultaneous anchoring of Ni nanoparticles and single-atom Ni on BCN matrix promotes efficient conversion of nitrate in water into high-value-added ammonia, *Chem. Eng. J.*, 2022, **433**, 133190.

19 L. Li, C. Tang, X. Cui, Y. Zheng, X. Wang, H. Xu, S. Zhang, T. Shao, K. Davey and S. Qiao, Efficient nitrogen fixation to ammonia through integration of plasma oxidation with electrocatalytic reduction, *Angew. Chem., Int. Ed.*, 2021, **60**, 14131–14137.

20 X. Zhao, X. Jia, Y. He, H. Zhang, X. Zhou, H. Zhang, S. Zhang, Y. Dong, X. Hu, A. V. Kuklin, G. V. Baryshnikov, H. Ågren and G. Hu, Two-dimensional BCN matrix inlaid with single-atom-Cu driven electrochemical nitrate reduction reaction to achieve sustainable industrial-grade production of ammonia, *Appl. Mater. Today*, 2021, **25**, 101206.

21 P. Huang, T. Fan, X. Ma, J. Zhang, Z. Chen and X. Yi, 3D Flower-Like zinc cobaltite for electrocatalytic reduction of nitrate to ammonia under ambient conditions, *ChemSusChem*, 2022, DOI: 10.1002/cssc.202102049.

22 J. Chen, Q. Zhou, L. Yue, D. Zhao, L. Zhang, Y. Luo, Q. Liu, N. Li, A. A. Alshehri, M. S. Hamdy, F. Gong and X. Sun, Co–NCNT nanohybrid as a highly active catalyst for the electroreduction of nitrate to ammonia, *Chem. Commun.*, 2022, **58**, 3787–3790.

23 Y. Wang, A. Xu, Z. Wang, L. Huang, J. Li, F. Li, J. Wicks, M. Luo, D. H. Nam, C. Tan, Y. Ding, J. Wu, Y. Lum, C. T. Dinh, D. Sinton, G. Zheng and E. H. Sargent, Enhanced nitrate-to-ammonia activity on copper–nickel alloys via tuning of intermediate adsorption, *J. Am. Chem. Soc.,* 2020, **142**, 5702–5708.